The First Chapters of Our Cosmic History with JWST
Proceedings IAU Symposium No. 391, 2025
T. Nanayakkara & M. Maseda, eds.
doi:10.1017/S1743921324002382

The origin of unusual chemical abundances from the JWST

Dyna Ibrahim and Chiaki Kobayashi

Centre for Astrophysics Research, University of Hertfordshire
email: d.ibrahim3@herts.ac.uk

Abstract. To understand the formation and evolution of the Universe, it is crucial to understand how and when the first stars formed. The latest observational data reveal unprecedented information about the chemical enrichment of the early Universe, which seems to behave differently from the local Universe. The first stars, being very massive, enrich their metal-poor environment in an uncertain way. In order to predict the abundances of the first galaxies, we include nucleosynthesis yields from Population III stars up to $300M_{\odot}$, including faint supernovae, Wolf-Rayet (WR) stars and Pair-Instability Supernovae (PISN) into our state-of-the-art hydrodynamical cosmological simulations. Our code (based on Gadget-3) also includes the latest nucleosynthesis yields from population II stars (from Kobayashi et al. 2020) for all stellar mass ranges. We predict the chemical abundance evolution of galaxies for different elements from the early Universe to the local Universe. We first test the modelling of stellar feedback by comparing the observed evolution of mass–metallicity relations (MZR) and metallicity gradients of the interstellar medium. We then compare our model including Population III stars with observational data from the James Web Space Telescope (JWST). For elemental abundances, we find that the N/O abundance gives a systematically higher value, comparable to the observational data of very high-redshift galaxies such as GN-z11.

Keywords. galaxies: abundances – galaxies: formation – galaxies: evolution – methods: numerical.

1. Introduction

Recent observational data from the James Webb Space Telescope (JWST) pushed the barriers to our understanding of galaxy formation and evolution in the early Universe. These discoveries have shown surprisingly strong emission lines in very high-redshift galaxies, for instance, the Nitrogen-to-Oxygen abundance ratios of the galaxy GN-z11 at $z = 10.6$ (Bunker et al. 2023). Other galaxies have then been observed to show similar features (e.g., Marques-Chaves et al. 2024, $z = 8.68$; Isobe et al. 2023, $z = 6.23$; Topping et al. 2024a, $z = 6.1$; Topping et al. 2024b, $z = 7.04$; Castellano et al. 2024, $z = 12.34$; Schaerer et al. 2024, $z = 9.3$).

There are already various scenarios trying to explain the observed high N/O ratio. For example, using a correlation with globular clusters (e.g. Charbonnel et al. 2023; Senchyna et al. 2024), while others suggest that the enrichment comes from supermassive stars (Nagele and Umeda 2023; Nandal et al. 2024). In the very early Universe, the properties of the first stars may be very different. This includes the stellar mass function (which can be top-heavy) and the nucleosynthesis yields. Another hypothesis is from Kobayashi and Ferrara (2024) who presented chemical evolution models that can explain the observations with Wolf-Rayet stars and intermittent star formation.

However, GN-z11 is already an evolved galaxy with stellar mass of $\sim 10^9$ $M_\odot$, and to understand the formation and evolution of these galaxies, it is important to simulate them in a cosmological context. This work is the very first attempt to include these chemical enrichment sources self-consistently in cosmological hydrodynamical simulations.

2. Method

We use cosmological hydrodynamical simulations based on the `GADGET-3` code (Springel et al. 2005) in a comoving $25h^{-1}$Mpc cubic box with periodic boundary conditions. The number of gas and dark matter particles are $N_{\rm gas} = N_{\rm DM} = 320^3$, with mass $M_{\rm gas} = 9.34 \times 10^6$ $M_\odot$ and $M_{\rm DM} = 5.1 \times 10^7$ $M_\odot$. We use the same initial conditions and physical processes as in Ibrahim and Kobayashi (2024): metallicity-dependent radiative cooling, star formation, stellar feedback, black hole physics (Kobayashi 2004; Taylor and Kobayashi 2014), and chemical enrichment (Kobayashi et al. 2020). One of the most uncertain phenomena remains supernova feedback.

To constrain supernova feedback in our simulations, we study its impact on the mass–metallicity relation and metallicity radial gradients. In Ibrahim and Kobayashi (2024), we studied the dependence of mass–metallicity relations (MZRs) on supernovae feedback in a $10h^{-1}$Mpc volume up to $z = 3$, for that we implemented and compared four models of supernova feedback to our cosmological simulations: the thermal feedback which consists of pure thermal energy distributed to the neighbour gas particles, the stochastic feedback (similar to Dalla Vecchia and Schaye 2012) stochastically distributing thermal energy to a random number of particles (we use the probability parameter f=50), the kinetic feedback (Navarro and White 1993) partially converting the thermal energy into kinetic energy (the fraction parameter f=1%), and the mechanical feedback (Hopkins et al. 2014) which accounts the physics during the different phases of the supernova expansion (the fraction parameter f=1%).

In Section 3, we constrain supernova feedback in our cosmological simulations using stellar and gas-phase MZRs up to $z = 5$, as well as gas-phase metallicity gradients (Ibrahim and Kobayashi, in prep). Section 4 presents our first results for elemental abundances with our new nucleosynthesis yields including Population III (Pop III) stars.

3. Metallicity evolution

The top panels of Figure 1 show the V-band luminosity-weighted stellar MZRs for the thermal (blue, solid line), stochastic (orange, dash-dotted), kinetic (green, dashed) and mechanical (red, dense dash-dotted) feedback models from $z = 0.7$ to 5. The lines show the medians of all individual galaxies identified in our simulations, while the shaded areas show the 1σ scatter. The dotted lines and symbols are observational data. We use a solar metallicity $Z_\odot = 0.015$.

At $z = 0.7$, our kinetic model seems too strong and does not produce enough metals to explain the observations (see Ibrahim and Kobayashi 2024). Despite no overlap in the mass range, this model seems consistent with data from Gallazzi et al. (2014). However, we note its large error bar of ~ 1 dex. The thermal and stochastic models overproduce metals compared to the mechanical feedback for low-mass galaxies ($M < 10^{10} M_\odot$), which result in significantly higher metallicities than in Gallazzi et al. (2014) for massive ones. These models suggest that the stellar mass–metallicity relation has not significantly evolved between $z \sim 0.7$ and $z \sim 3$, at least at the massive end, contrary to the kinetic model. At $z = 3$, the UV observations from Cullen et al. (2019) for Fe abundances are shifted by +0.5 dex taking account of [O/Fe] and seem to nicely match our kinetic model, but again, we note the large error bar of ~ 1 dex for this model. At $z = 5$, the kinetic model only produces two low-mass galaxies, which explains the absence of MZR for this

https://doi.org/10.1017/S1743921324002382 Published online by Cambridge University Press

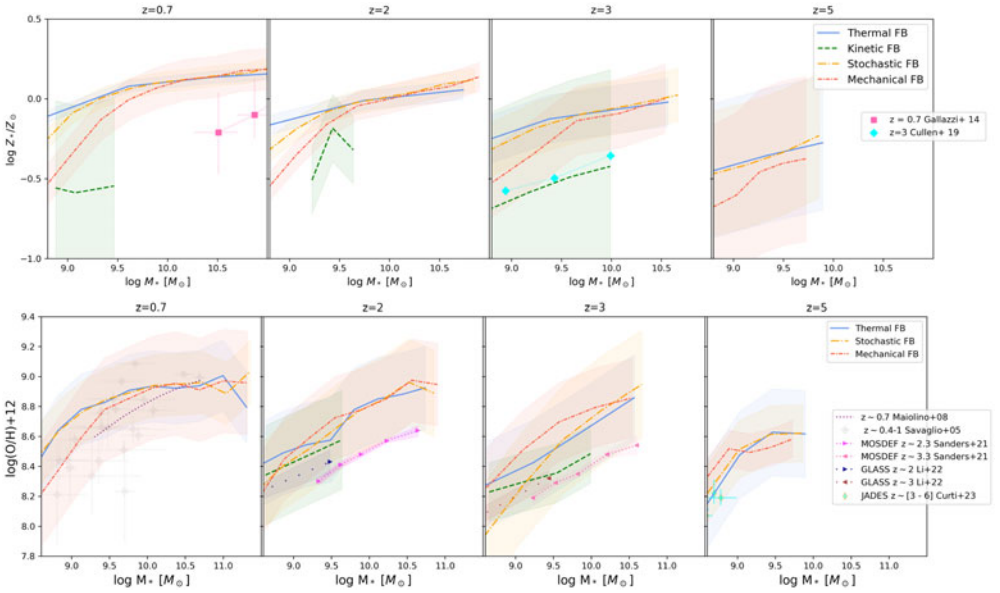

Figure 1. Top panel: Redshift evolution of the luminosity-weighted stellar MZRs of galaxies for the thermal (blue, solid), stochastic (orange,dashed), and mechanical (red, dash-dotted) feedback models. The lines are for the medians, and the shaded areas show the 1σ scatter. Observational data are taken from Gallazzi et al. 2014 ($z = 0.7$), and Cullen et al. 2019 ($z = 3$, with $+0.5$ dex shift for [O/Fe]). Bottom panel is the same but for the SFR-weighted gas-phase MZRs. Observational data (dotted with different symbols) are from Sanders et al. 2021 ($z \sim 2-3$), Li et al. 2022 ($z \sim 2-3$), and Curti et al. 2024 ($z \sim 3-6$).

model. At high redshifts, we retrieve the mass–metallicity relation for thermal, stochastic and mechanical models, with the metallicity at a given mass being lower by ~ 0.4 dex from $z = 5$ to $z = 0.7$. The thermal feedback always produces slightly more metals than the other models for $M < 10^{10} M_{\odot}$, and the kinetic feedback results in significantly lower stellar metallicities than in the other models. Overall, the supernova feedback has a more significant impact on the metallicity at the low-mass end, where low-mass galaxies eject more metals into the intergalactic medium (Kobayashi et al. 2007).

The bottom panel of Figure 1 is the same but for the gas-phase MZRs with SFR-weighted gas oxygen abundance from $z = 0.7$ to 5 for the same four feedback models (see Ibrahim and Kobayashi 2024 for the details). The lines show the medians of individual galaxies in our simulations. The dotted lines and symbols represent observational data at various redshifts, some of which may be suffered by the small sample as already discussed. All observational data have been converted for the Kroupa IMF.

At $z = 0.7$, our kinetic feedback has no star-forming galaxies, which explains the absence of MZR. While our mechanical feedback model most agrees with observed data from Maiolino et al. (2008) and Savaglio et al. (2005). With this resolution, we have a limited sample, but we still retrieve the MZR at all redshifts with thermal, stochastic and mechanical. At higher redshifts, the metallicities at a given mass are considerably lower for the kinetic feedback due to the suppression of star formation, leading to few metal-poor low-mass galaxies. At $z = 5$, the sample of galaxies with the kinetic feedback is too limited to show the MZR. We find a significant evolution from $z \sim 5$ to 0.7 for the gas-phase MZR in the the thermal, stochastic and mechanical feedbacks (~ 0.2 dex). At higher redshifts, the MOSDEF (Sanders et al. 2021) and GLASS survey with NIRISS slitless spectroscopy on JWST (Li et al. 2022) showed ~ 0.1 and ~ 0.07 dex evolution from

https://doi.org/10.1017/S1743921324002382 Published online by Cambridge University Press

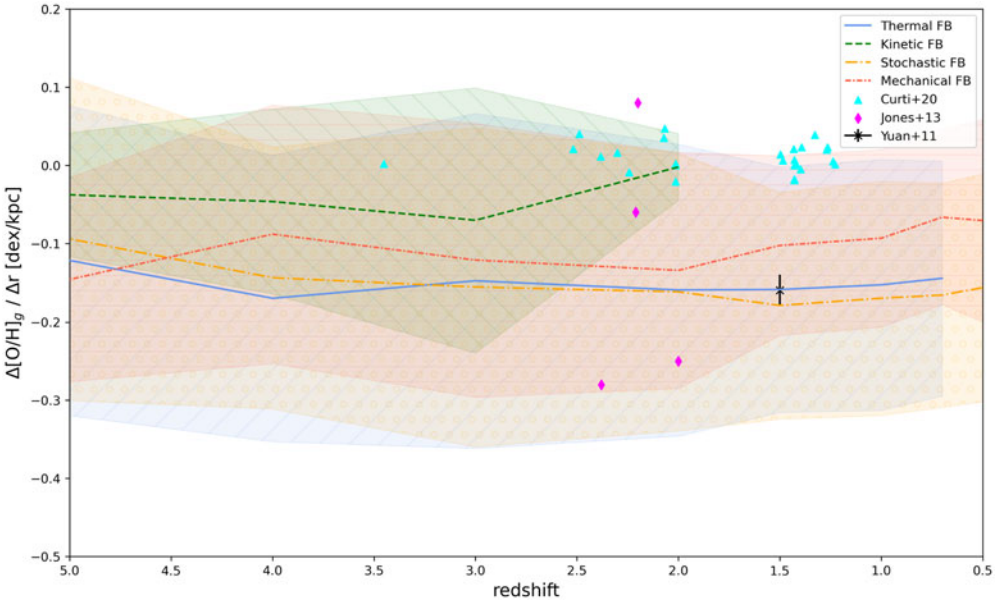

Figure 2. SFR-weighted gas-phase metallicity gradient as a function of redshift, for all galaxies in our simulations with the thermal (blue solid line), kinetic (green dashed), stochastic (orange dash-dotted), and mechanical (red dense dash-dotted) feedback models. The shaded areas are 1σ scatter. The symbols are observational data from Yuan et al. 2011 (black cross) using AO-assisted spectroscopy OSIRIS on Keck II on a face-on spiral galaxy at $z \sim 1.5$, Jones et al. 2013 (magenta diamonds) using AO-assisted spectroscopy OSIRIS on Keck on gravitationally lensed systems, and Curti et al. 2020 (cyan triangle) using KMOS KLEVER survey on 42 gravitationally lensed galaxies.

$z \sim 2$ to $z \sim 3$, respectively, which is larger than in all our models (~ 0.07 dex), except for the kinetic. The kinetic feedback model fits well with the laters, but as discussed previously, this model is underproducing stars, so this matching does not necessarily support the kinetic feedback of supernovae. At $z = 5$, the JADES survey (Curti et al. 2024) with JWST/NIRSpec at $3 < z < 6$ for low mass galaxies show a nice match with our thermal model.

Figure 2 shows the SFR-weighted gas-phase metallicity gradients as a function of redshift for all our galaxies with the thermal (blue solid line), kinetic (green, dashed), stochastic (orange, dash-dotted), and mechanical (red, dense dash-dotted) feedback models. The gradient is measured within $2R_e$ where R_e is the effective radius of each galaxy. We show the redshift evolution from $z = 5$ up to $z = 0.5$ for the stochastic and mechanical models, to $z = 0.7$ for the thermal model, and to $z = 2$ for the kinetic feedback which stops forming stars after $z = 2$ with this resolution. The shaded areas show the 1σ scatter.

The symbols represent observational data from Curti et al. 2020 (cyan triangle), Yuan et al. 2011 (black cross), Jones et al. 2013 (magenta diamonds). These observational data nicely match our gradients with the kinetic feedback near $z \sim 2$. The gradients with the mechanical feedback is flatter than those with thermal and stochastic feedback, but with all three supernovae feedback models, the gradients remain mostly negative at all redshifts, suggesting that galactic centers are more metal-rich than the outskirts. A detailed analysis of both of the stellar and gas-phase metallicity gradients will be discussed in Ibrahim and Kobayashi, in prep.

https://doi.org/10.1017/S1743921324002382 Published online by Cambridge University Press

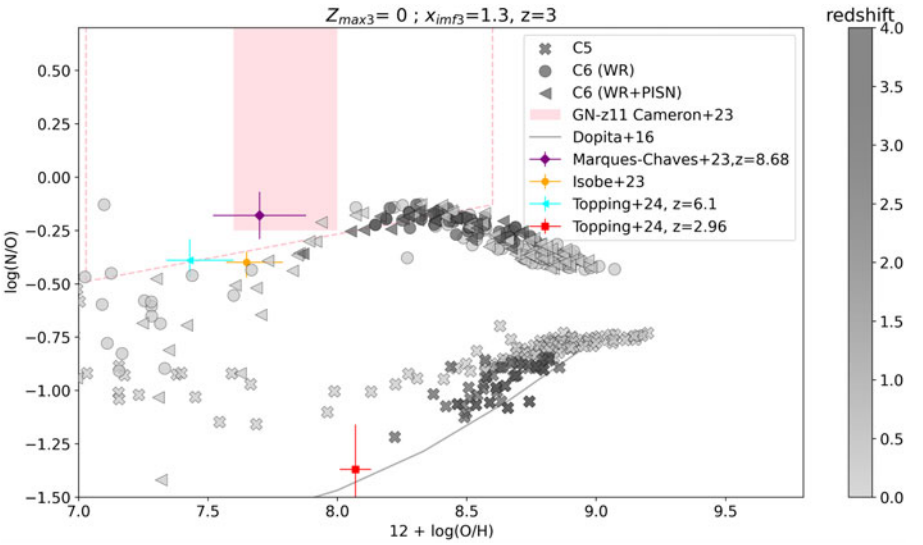

Figure 3. The evolution of SFR-weighted gas-phase N/O abundance ratios compared to oxygen abundances with Pop III nucleosynthesis yields from WR (circles), WR and PISN (triangles) and without (cross) (including faint supernovae)

4. Elemental abundance

To explain the N/O ratios of very high redshift galaxies, we use the latest nucleosynthesis yields from Kobayashi et al. 2020, but including PISN (Takahashi et al. 2018), WR stars (Limongi and Chieffi 2018), and faint supernovae for Pop III stars, as in Kobayashi and Ferrara (2024). We have varied many parameters for the Pop III contributions in our simulations but show the abundance ratios with three different cases in Figure 3, all with a constant Kroupa IMF slope (Kroupa 2008) between the lower and upper mass limits ($[m_\ell, m_\mathrm{u}]$). For the comparison to our previous "C5" simulations in Section 3, we use thermal feedback only.

In Figure 3 we show our simulation C5 without nucleosynthesis yields from PISN or WR stars (cross symbols) from $z = 0$ (dark gray), to $z = 4$ (light gray). This gives a nice match with local observational data (solid line) from Dopita et al. (2016). This observed local relation has been explained as follows. (i) The plateau at low metallicities is caused by rotating massive stars in one-zone galactic chemical evolution models (Chiappini et al. 2006), *or* inhomogeneous enrichment from asymptotic giant branch (AGB) stars in cosmological simulations as explained in Vincenzo and Kobayashi (2018). (ii) The increasing trend toward higher metallicities is caused by the metallicity dependence of N yields in all mass range of stars *and* the delayed enrichment from AGB stars.

We also show our model C6 including Pop III star nucleosynthesis yields from rotating WR stars (circles) with [0.01,120]$\mathrm{M}_\odot$, and another model C6 including both rotating WR stars and PISNe (triangles) with [15, 300]$\mathrm{M}_\odot$. These C6 simualtions produce a significantly different N/O ratios, mainly caused by the rotating star models. In massive stars, rotation enhances mass loss through stellar winds, ejecting elements like nitrogen and carbon and increasing the number of WR stars (e.g. Limongi and Chieffi 2018). As a result, the presence of rotating WR stars (at all metallicities) enhances N/O abundance ratios in galaxies (at all redshifts). The stellar rotation highly impacts the chemical enrichment history of galaxies, much more than the presence of PISNe.

https://doi.org/10.1017/S1743921324002382 Published online by Cambridge University Press

4.1. *Conclusion*

We show our cosmological hydrodynamical simulations that include the latest nucleosynthesis yields. Our main findings are:

• Our analysis of MZRs and metallicity gradients evolution suggest that mechanical feedback gives the best match to the local observations, although stronger supernovae feedback such as our kinetic model may be required at $z > 2$.

• Nucleosynthesis yields from rotating WR stars in our simulations can enhance N/O abundance ratios in galaxies, and the metallicity dependence of stellar rotations might be required to explain observations at both low and high redshifts.

References

Andrew J. Bunker et al. *A&A*, 677:A88, September 2023. doi: 10.1051/0004-6361/202346159
Marco Castellano et al. *ApJ*, 972(2):143, September 2024. doi: 10.3847/1538-4357/ad5f88
C. Charbonnel et al. *A&A*, 673:L7, May 2023. doi: 10.1051/0004-6361/202346410
C. Chiappini et al. *A&A*, 449(2):L27–L30, April 2006. doi: 10.1051/0004-6361:20064866
F. Cullen et al. *MNRAS*, 487(2):2038–2060, August 2019. doi: 10.1093/mnras/stz1402
Mirko Curti et al. *MNRAS*, 492(1):821–842, February 2020. doi: 10.1093/mnras/stz3379
Mirko Curti et al. *A&A*, 684:A75, April 2024. doi: 10.1051/0004-6361/202346698
Claudio Dalla Vecchia and Joop Schaye. *MNRAS*, 426(1):140–158, October 2012
Michael A. Dopita et al. *Ap&SS*, 361:61, February 2016. doi: 10.1007/s10509-016-2657-8
Anna Gallazzi et al. *ApJ*, 788(1):72, June 2014. doi: 10.1088/0004-637X/788/1/72
Philip F. Hopkins et al. *MNRAS*, 445(1):581–603, November 2014. doi: 10.1093/mnras/stu1738
Dyna Ibrahim and C. Kobayashi. *MNRAS*, 527(2):3276–3290, January 2024. doi: 10.1093/mnras/stad3313
Yuki Isobe et al. *ApJ*, 959(2):100, December 2023. doi: 10.3847/1538-4357/ad09be
Tucker Jones et al. *ApJ*, 765(1):48, March 2013. doi: 10.1088/0004-637X/765/1/48
Chiaki Kobayashi. *MNRAS*, 347(3):740–758, January 2004. doi: 10.1111/j.1365-2966.2004.07258.x
Chiaki Kobayashi and Andrea Ferrara. *ApJ*, 962(1):L6, February 2024. doi: 10.3847/2041-8213/ad1de1
Chiaki Kobayashi, Volker Springel, and Simon D. M. White. 376(4):1465–1479, mar 2007
Chiaki Kobayashi, Amanda I. Karakas, and Maria Lugaro. *ApJ*, 900(2):179, September 2020
Pavel Kroupa. In Sverre J. Aarseth, Christopher A. Tout, and Rosemary A. Mardling, editors, volume 760, page 181, 2008. doi: 10.1007/978-1-4020-8431-7_8
Mingyu Li et al., 2022
Marco Limongi and Alessandro Chieffi. *ApJS*, 237(1):13, July 2018. doi: 10.3847/1538-4365/aacb24
R. Maiolino et al. *A&A*, 488(2):463–479, September 2008. doi: 10.1051/0004-6361:200809678
R. Marques-Chaves et al. *A&A*, 681:A30, January 2024. doi: 10.1051/0004-6361/202347411
Chris Nagele and Hideyuki Umeda. *ApJ*, 949(1):L16, May 2023. doi: 10.3847/2041-8213/acd550
Devesh Nandal et al. *A&A*, 683:A156, March 2024. doi: 10.1051/0004-6361/202348035
J. F. Navarro and S. D. M. White. *MNRAS*, 265:271, November 1993. doi: 10.1093/mnras/265.2.271
Ryan L. Sanders et al. *ApJ*, 914(1):19, June 2021. doi: 10.3847/1538-4357/abf4c1
S. Savaglio et al. *ApJ*, 635(1):260–279, December 2005. doi: 10.1086/497331
D. Schaerer et al. *A&A*, 687:L11, July 2024. doi: 10.1051/0004-6361/202450721
Peter Senchyna et al. *ApJ*, 966(1):92, May 2024. doi: 10.3847/1538-4357/ad235e
Volker Springel et al. *MNRAS*, 361(3):776–794, August 2005. doi: 10.1111/j.1365-2966.2005.09238.x
Koh Takahashi et al. *ApJ*, 857(2):111, April 2018. doi: 10.3847/1538-4357/aab95f
P. Taylor and C. Kobayashi. *MNRAS*, 442(3):2751–2767, August 2014. doi: 10.1093/mnras/stu983
Michael W. Topping et al. *MNRAS*, 529(4):3301–3322, April 2024a. doi: 10.1093/mnras/stae682

Michael W. Topping et al. *arXiv e-prints*, art. arXiv:2407.19009, July 2024b. doi: 10.48550/arXiv.2407.19009

F. Vincenzo and C. Kobayashi. *MNRAS*, 478(1):155–166, July 2018. doi: 10.1093/mnras/sty1047

T. T. Yuan, L. J. Kewley, A. M. Swinbank, J. Richard, and R. C. Livermore. *ApJ*, 732(1):L14, May 2011. doi: 10.1088/2041-8205/732/1/L14